CERN-INTC-2016-059 / INTC-P-487
02/11/2016

EUROPEAN ORGANIZATION FOR NUCLEAR RESEARCH

Proposal to the ISOLDE and Neutron Time-of-Flight Committee

Neutron unbound single particle states in ^{133}Sn from the beta decay of ^{133}In

7/10/2016

M. Madurga[1], R.Grzywacz[1,2], S.V. Paulauskas[1], T.T. King[1], A. Algora[3], A.N. Andreyev[4], D.W. Bardayan[5], T. Berry[6], M.J.G. Borge[7], N.T. Brewer[2], J. Cederkall[8], A. Fijalkowska[9], A. Gottardo[10], L. Fraile[11], H.O.U. Fynbo[12], K.C. Goetz[1],L. Harkness-Brennan[13], A. Illana[14], S.V. Ilyushkin[15], D. Joss[13], D. Judson[13], K. Kolos[16], T. Kurtukian-Nieto[17], A. Korgul[18], A. Lepallieur[9], R. Licâ[19,20], N. Marginean[20], R. Marginean[20], C. Mazzocchi[18], C. Mihai[20], K. Miernik[18], A.I. Morales[3], E. Nacher[3], A. Negret[20], C.R. Nita[20], B. Olaizola[21], R.D. Page[13], S. Pascu[20], W.A. Peters[22], M. Piersa[18], Z. Podolyak[6], M. Ramdhane[23], B.C. Rasco[2], K. P. Rykaczewski[2], J. Snall[8,19], C. Sotty[20], D. Stracener[2], Marek Stryjczyk[14], S. Taylor[1], O. Tengblad[7], P. Van Duppen[14], D. Walter[9], N. Warr[24], H. de Witte[15], Y. Xiao[1]

[1]Dept. of Physics and Astronomy, University of Tennessee, Knoxville, Tennessee 37996, USA.
[2]Physics Division, Oak Ridge National Laboratory, Oak Ridge, Tennessee 37830, USA.
[3]Instituto de Física Corpuscular, Edificio de Institutos de Paterna, E-46071 Valencia, Spain.
[4]Department of Physics, University of York, York YO10 5DD, United Kingdom.
[5]Institute for Structure and Nuclear Astrophysics, Department of Physics, Notre Dame, Indiana 46556, USA.
[6]Department of Physics, University of Surrey, Guildford, Surrey GU2 7XH, United Kingdom.
[7]Instituto de Estructura de la Materia, CSIC, E-28006 Madrid, Spain.
[8]Physics Department, Lund University, P. O. Box 118, SE-221 00 Lund, Sweden.
[9]Dept. of Physics and Astronomy, Rutgers University, New Brunswick, NJ 08903 USA.
[10]Institut de Physique Nucléaire, CNRS-IN2P3, 91406 Orsay Cedex, France.
[11]Universidad Complutense de Madrid, Avenida Complutense, E-28040 Madrid, Spain.
[12]Department of Physics and Astronomy, Aarhus University, 8000 Aarhus C, Denmark.
[13]Oliver Lodge Laboratory, Department of Physics, University of Liverpool, Liverpool, L69 7ZE, United Kingdom.
[14]KU Leuven, Instituut voor Kern-en Stralingsfysica, 3001 Leuven, Belgium.
[15]Department of Physics, Colorado School of Mines, Golden CO 80401.
[16]Lawrence Livermore National Laboratory, Livermore, California 94550, USA.
[17]Centre d'Etudes Nucléaires de Bordeaux Gradignan, CNRS/IN2P3, 33175 Gradignan Cedex, France.
[18]Faculty of Physics, University of Warsaw, PL 00-681 Warsaw, Poland.
[19]EP-division, CERN 1211, Geneva 23, Switzerland.
[20]"Horia Hulubei" National Institute for Physics and Nuclear Engineering, 077125 Bucharest-Măgurele, Romania.
[21]TRIUMF, 4004 Wesbrook Mall, Vancouver, British Columbia, Canada V6T 2A3.
[22]Joint Institute for Nuclear Physics and Applications, Oak Ridge, Tennessee 37831, USA.
[23]LPSC, Université Joseph Fourier Grenoble 1, CNRS/IN2P3, F-38026 Grenoble Cedex, France.
[24]Institut für Kernphysik, Universität zu Köln, Germany.

Spokesperson(s): Miguel Madurga Flores (Miguel.madurga@gmail.com)
Robert Grzywacz (rgrzywac@utk.edu)
Local contact: Razvan Lica (razvan.lica@cern.ch)

Abstract

We propose to measure the excited neutron-unbound states in ^{133}Sn populated in beta decay of ^{133}In. Ground ($9/2^+$) and ($1/2^-$) isomeric states of ^{133}In precursor will be laser-selected. Beta-delayed neutron emission will be observed using the newly commissioned ISOLDE Decay Station Neutron Detector (IDSND). Owing to the closed-core nature of ^{132}Sn, the nuclear structure properties of ^{133}Sn are determined by the simple configurations of single-particle/hole of shell model orbitals. While previous decay and direct reactions experiments established energies of neutron particle configurations outside ^{132}Sn, this proposal aims to detect excited hole states of ^{132}Sn core, which can be best studied in beta decay. The decay of ^{133}In provides a unique opportunity to investigate the population of both negative and positive parity states in ^{133}Sn. Allowed beta-decay transitions can only occur between the $\nu g_{7/2}$ and $\pi g_{9/2}$ orbitals, and this will be a dominant decay channel for the ground state of ^{133}In. Forbidden-type beta decays will dominate decay of the $1/2^-$ state although it will be active in both ground state and isomer decays. From the neutron spectroscopy, we will determine the position of the ^{132}Sn single particle configurations at the Fermi level of the Z=50 and N=82 shell closures. That includes neutron hole configurations involving $d_{3/2}$, $h_{11/2}$, $s_{1/2}$, $g_{7/2}$, $d_{5/2}$ and $g_{7/2}$ orbitals, and proton single-particle states $d_{5/2}$ and $g_{7/2}$.

Requested shifts: 13 shifts

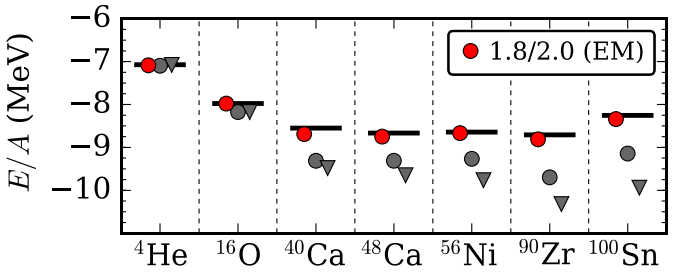

Figure 1. Calculated binding energy per nucleon for doubly-magic nuclei using chiral nucleon-nucleon and three-nucleon interaction[Hag16,Pap16] (red circles[Heb11], grey circles and triangles[Bin14]). A single interaction is now capable of reproducing experimental energies (black line) for all doubly-magic nuclei shown.

Introduction

The experiments on nuclei in regions close to doubly-magic species are essential to test the nuclear models involving spherical nuclear potential. Here, new theories are put to the test for the first time [Ots10,Wat14,Hag16] before any predictions can be made for more complicated systems. Decay spectroscopy, due to its intrinsic sensitivity is often a tool of choice to study those regions where doubly magic nuclei are also very exotic, such as: ^{48}Ca, ^{48}Ni,^{78}Ni, ^{100}Sn and ^{132}Sn. For the neutron rich cases, such as ^{132}Sn and ^{78}Ni, the structure of these nuclei is also entwined with the r-process nucleosynthesis, in a straightforward way, through decay properties, or more subtly, through the r-process sensitivity to the radiative neutron capture cross sections. The evolution of beta-decay half-lives and masses in isotopic/isotonic chains often reveals the effects of modifications of the nuclear interaction with changing neutron/proton number[Wie13,Xu14]. With increasing neutron/proton asymmetry the decay energy window (Q_β) grows in exotic regions and allowing for high-energy particle-unbound states to be populated, which are difficult to observe in experiments using nuclear reactions (see i.e. [Gre04,Per06]), either because of lack of rates or different selection rules. Moreover, the experimental beta-decay strength distribution offers a sensitive probe to nuclear structure, as it depends on the overlap between the mother wave function and the daughter states [Nac04,Mad16].

The region of nuclei around double magic ^{132}Sn has recently received considerable attention. The large energy gaps at the Z=50 and N=82 shell closures make ^{132}Sn the best example of a spherical core [Jon10]. This makes the region very attractive to study nuclear structure driven by single particle orbital evolution. Recently, many beams of Z<50 and N>82 are now available at ISOLDE and RIKEN [Tap14,Tap15,Lor15,Ata15,Jun16a,Jun16b,Lic16]. This region is characterized by large Q_β values and low neutron separation energies, making neutron spectroscopy an attractive tool to study their decays. This, however, considerably increases the experimental difficulty and partially explains the dearth of data in the region.

Nuclei around the neutron magic number N=82 also play an important role in the rapid neutron capture in astrophysical nucleosynthesis [Lor15]. In particular, the beta decay half-lives of even-even N=82 and N=84 Cd and Pd isotopes have been shown to have a large impact on the final abundances in calculations [Mum16]. The main allowed transitions determining both beta-decay half-lives populate 1+ states with a large $\nu g_{7/2} \rightarrow \pi g_{9/2}$ component, as those have the biggest matrix elements and are energetically favored [Zhi13]. Studying the decay of ^{133}In offers a unique opportunity to stablish the microscopic foundations of these transitions due to the simplicity of the ^{133}Sn configurations. As we will demonstrate later the beta-decay of ^{133}In is dominated by pure single-particle $\nu g_{7/2} \rightarrow \pi g_{9/2}$ transition. The determination of the experimental strength of this transition will provide a benchmark for calculations in the entire region.

Recently, progress has been made using the shell model to calculate nuclei in the Z<50 and N>82 region southeast of ^{132}Sn [Jun16b]. The low energy excitation scheme of ^{131}In was successfully reproduced using the $\pi(f_{5/2}pg_{9/2})\nu(f_{7/2}ph_{9/2}f_{5/2}i_{13/2})$ valence space. However, one must notice that half-life calculations in this region must include neutron single-hole states in the N<82 orbitals to account for the dominating Gamow-Teller transitions. Models capable of calculating the structure and decay strength around mid-mass and heavy doubly-magic nuclei from first-principles computations are now being developed (see Fig. 1.) [Hag16,Pap16]. The experimental neutron single-particle and single-hole energies in ^{133}Sn will provide a strong verification of their accuracy and their applicability for nuclei farther away from stability.

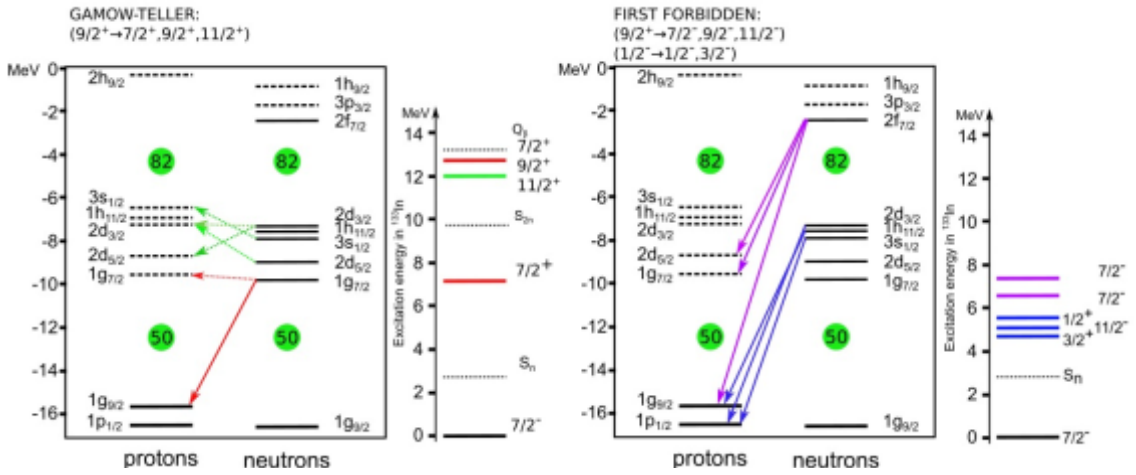

Figure 1. Single particle orbitals relevant for the decay of ^{133}In. Gamow-Teller decay will proceed mainly via $g_{9/2}$ to $g_{7/2}$ transformation. The resulting excited state (re line) will be determined by the position of the $g_{7/2}$ neutron orbital with respect to Fermi energy (left). The forbidden decays can involve transition between states of different parity. They have smaller transition matrix elements but are at lower excitation energies (right).

Beta-Decay of ^{133}In

The beta decay half-life of ^{133}In ($T_{1/2}$=163(7) ms) has only been reported in two previous experiments [Hof96, Lor15]. The particle-bound states in ^{133}Sn, corresponding to neutron single-particle orbitals, were initially observed in both the decay of ^{133}In and the beta-delayed neutron branch of ^{134}In [Hof96]. Hoff and collaborators also measured the delayed neutron emission after the decay of ^{133}In. The largest intensity neutron transition observed at 1.26 MeV was assigned to the forbidden decay of the $9/2^+$ ground state into the $11/2^-$ state, corresponding to the $(h_{11/2})^{-1}$ orbital. Other neutron transitions at higher energies were present in their spectrum but they were not discussed. A $13/2^+$ state, corresponding to the $i_{13/2}$ neutron orbital, has been hypothesized to be neutron unbound, but has not yet been observed. This is not unexpected, as beta decay feeding this state from the $9/2^+$ g.s. of ^{133}In directly would be second-forbidden. It would be at least 2 orders of magnitude smaller than any other beta-decay transitions in the decay of the ground state.

Figure 1 shows the shell-model picture of the ^{133}In decay. The large N=82 (~6 MeV) and Z=50 (~5 MeV) shell gaps constrain the number of available excited states configurations involved in beta decays. The left panel shows all possible Gamow-Teller (GT) decay transitions. The dominant $\nu g_{7/2} \rightarrow \pi g_{9/2}$ transition corresponds to the daughter in a $(\nu g_{7/2}^{-1} f_{7/2}^{+2})$ configuration. The excitation energy thus follows the relative spacing between $\nu g_{7/2}$ and $\nu f_{7/2}$ orbitals, which is larger than N=82 shell-gap and exceeds neutron separation energy (Sn=2.4 MeV [Wan12]) in ^{132}Sn. The other possible GT transformations will populate proton spin-orbit partner states across Z=50 closed shell. They will have excitation energies as large as 10 MeV from the approximate sum of proton and neutron shell gap energies (green). Of course, forbidden transitions offer more decay paths which can connect with low excitation energy states in the daughter. Here we will consider only the first-forbidden type, which occur between orbitals of opposite parities and ΔJ=0,1. We also take into account that the electron-neutrino phase space favors decay to low excitation energies in the daughter. Thus, the most likely configurations populated in first-forbidden decay will correspond to orbitals close to the Fermi surfaces of the Z=50 and N=82 shells. Considering both GT and first forbidden transitions feeding unbound states in ^{133}Sn, we expect resulting neutron emission to be dominated from emission from the 7/2+ GT state and several weaker transitions corresponding to emission from neutron-hole states at the fermi surface of the N=82 shell and proton single particle states just above the Z=50 shell.

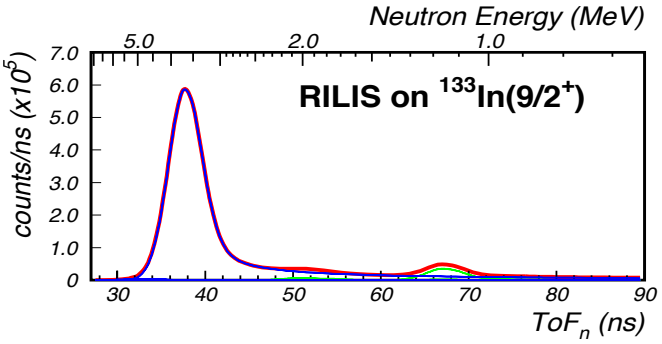

Figure 2: Simulation of the expected neutron spectra when selecting the decay of ^{133}In ground state using RILIS. The dominating peak (blue line) corresponds to neutrons emitted from the $\nu(g_{7/2})^{-1}f_{7/2}^{+2}$ state populated by allowed GT decay of the ground state. The neutron emission from states populated in forbidden decay (green line) can be seen at~ 50 and ~70 ns, corresponding to $\pi(g_{7/2},d_{5/2})^{+1}$ and $\nu h_{11/2}^{-1}$configurations respectively.

In order to verify the predictions for GT transformation, we performed a shell-model calculation of ^{133}In decay using ν-$(g_{7/2}d_{5/2}s_{1/2}h_{11/2}d_{3/2})$ π-$(f_{5/2}p_{3/2}p_{1/2}g_{9/2})$ valence space using the *jj99apn* set of interactions [Bro14] and recommended single particle energies. In order to enable calculations for the decay of N=84 nucleus ^{133}In, $\nu f_{7/2}$ valence orbital was added and a hybrid interaction was constructed in a similar manner as was shown in [Als16,Mad16]. In order to make the calculations tractable, in both ^{133}In and ^{133}Sn, two neutrons were blocked in the $f_{7/2}$ orbital as they do not play a role in GT decay due to the lack of energetically available spin-orbit partner proton orbital. As was deduced from simple analysis of Fig. 1 the main GT decay is expected to be dominated by the $\nu g_{7/2} \rightarrow \pi g_{9/2}$ transition. Due to the small fragmentation predicted for states in ^{133}Sn due to its proximity to ^{132}Sn, allowed decays should occur only between states with pure $\nu g_{7/2}$ and $\pi g_{9/2}$ configurations. Indeed, our model predicts one single dominating transition at 6.4 MeV, corresponding to the ^{132}Sn $(\nu g_{7/2}^{-1}f_{7/2}^{+2})$ configuration coupled to $7/2^+$. The other two predicted GT transitions correspond to states in ^{132}Sn of the same $(\nu g_{7/2}^{-1}f_{7/2}^{+2})$ configuration coupled to $9/2^+$ and $11/2^+$ respectively, but much smaller transition elements are predicted due to the reduced overlap with the ^{133}In ground state wave function. The strength of the forbidden-type transitions populating $\nu(d_{3/2}, h_{11/2}, s_{1/2})^{-1}f_{7/2}^{+2}$ configurations in ^{133}Sn can be deduced from systematics. Comparable transitions were identified in ^{121}In with $log(ft)_{1/2^-\rightarrow 3/2^+}=6.7$ and $log(ft)_{1/2^-\rightarrow 1/2^+}=6.22$, and in ^{123}In with $log(ft)_{9/2^+\rightarrow 11/2^-}=6.18$ [Sin98]. The configurations of proton excited states across the Z=50 shell $\pi(g_{7/2},d_{5/2})^{+1}\nu(f_{7/2})$ will couple to multiplets including states of $J=7/2^-,9/2^-,11/2^-$ parity, which will be populated in first-forbidden type beta transitions. In those cases, we assume a *log(ft)* value of 6.18 from the transition in ^{123}In mentioned above.

Figure 2 shows the expected response of IDSND to the neutron spectrum obtained from the shell model calculation of the beta-decay of ^{133}In and its $1/2^-$ isomer presented in the previous section. The intensity was calculated from the expected relative yields using narrowband RILIS to select the ground state and isomer individually (see next section). The IDSND time-of-flight response was simulated using Geant4 code and folding the experimental resolution described later. The neutron emission is dominated by the large GT transition to an excited state at 6.4 MeV (4 MeV neutron emission), corresponding to the $(\nu g_{7/2}^{-1}f_{7/2}^{+2})$ configuration coupled to $7/2^+$ mentioned above. The smaller GT transitions at higher energies correspond to the same $\nu g_{7/2}^{-1}$ configuration coupled to $9/2^+,11/2^+$. Comparing the experimental ^{133}In GT strength, and the ones measured for ^{130,132}Cd (ISOLDE experiment IS600), with calculations will provide critical information about specific GT quenching factors needed in this region, as they are related to the pure transformation of the $g_{7/2}$ neutron in a $g_{9/2}$ proton. This will be an essential feedback for the models aiming to predict beta decay lifetimes for very neutron rich nuclei.

The previously published ^{133}In beta-delayed neutron spectrum [Hof96] shows a small peak at ~ 4 MeV, but it is not as dominating as expected from our calculations. However, ^{3}He ionization chambers have notoriously small efficiency for high-energy neutrons [Fra77]. By using plastic scintillators, we can achieve a much more uniform efficiency at high energies (see next section). This was crucial in the observation by IDSND's sister detector VANDLE of high-energy neutron emission in ^{84}Ga owing to excitations of deep ^{78}Ni core states [Mad16].

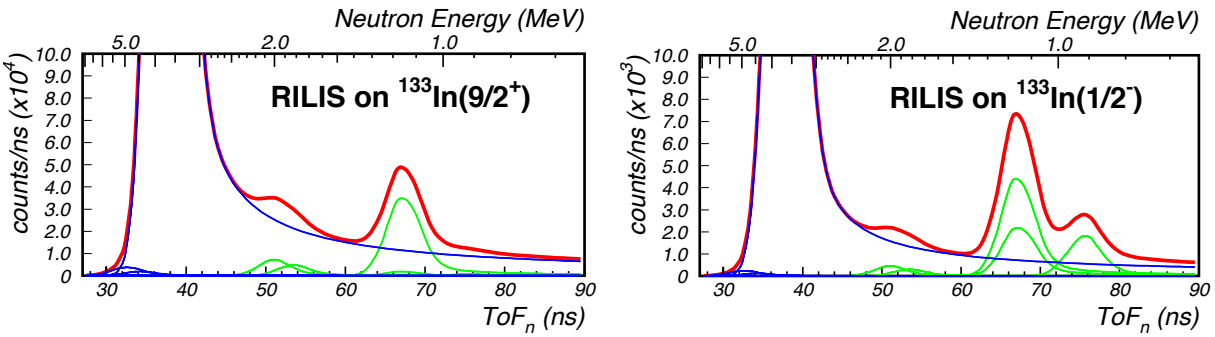

Fig 3: (left) Regions of neutron TOF spectrum from Fig. 2 zoomed in the neutron emission from the $\nu(h_{11/2})^{-1}$ state. A small component coming from off-resonance isomer decay can be seen. (right) Simulation of the decay of the ^{133}In 1/2$^-$ isomer. The neutron emission from the $\nu(d_{3/2},s_{1/2})^{-1}$ states is now enhanced compared to the off-resonance transition from the $\nu(h_{11/2})^{-1}$.

The neutron transitions at ~ 1 MeV in Fig. 3 left and right panels correspond to emission from states populated in forbidden decay to the single-hole $d_{3/2}$, $h_{11/2}$, $s_{1/2}$ states. In those cases, spin-parity rules strongly inhibit the population of the $3/2^+,1/2^+$ states from the $9/2^+$ ground state. We therefore expect from our calculations that the relative intensity of this neutron transition to be heavily influenced when the RILIS is used to selectively ionize nuclei in the ground state versus the isomeric state. Assuming the time resolution expected from previous measurements (see next section), we will be able to resolve the low energy transition, in this case from the $(d_{3/2})^{-1}$ state, from the other two. The measurement proposed here will allow us to experimentally determine the position of the $(vg_{7/2})^{-1}$ pure-single hole state relatively with the $\nu(d_{3/2}, h_{11/2}, s_{1/2})^{-1}$ and $\pi(g_{7/2},d_{5/2})^{+1}$ configurations.

Technical Aspects

The experiment will be instrumented at the ISOLDE Decay Station using its standard set of 4 clover detectors, ~4% efficiency at 1 MeV, the IDS in-vacuum beta detector, 90% electron detection efficiency, and the newly commissioned IDS Neutron Detector (see Fig. 4). IDSND consists of 26 individual detector modules placed in a custom-built support frame drawing an arch for a Time-Of-Flight path of 100 cm. Each detector module is made of a single 3x6x120 cm^3 EJ-200 plastic scintillator bar, wrapped in aluminized Mylar for light-tightness, and capped by 2 Hamamatsu photomultipliers at each end. Using two PMT tubes increases light collection and allows for position sensitivity along the module axis. The efficiency of IDSND modules was calibrated using a ^{252}Cf source [Pet16] to be about 40% at 1 MeV (see Fig 5). The angular acceptance for 26 bars at 100 cm is Ω=14.9% of 4π, and using 90% beta efficiency the total efficiency of the array is between 3-7%.

The time resolution of IDSND is determined by a combination of several factors. The intrinsic resolution 2ns at 1 MeV is due to the uncertainty in the position of the neutron interaction over the 3 cm module thickness and corresponds to 6% uncertainty in energy determination. The uncertainty is combined with the time resolution of the photomultipliers of the neutron and beta detectors. This composite resolution was experimentally determined during the commissioning run of IDSND from the width of the gamma response and was measured to be 1.75 ns on average. This resolution was implemented in the detector response simulations presented in this proposal, Fig. 2 and Fig. 3. The exact resolution and response of IDSND will be determined with a ^{17}N online calibration source. Nitrogen-17 is an excellent source for neutron detectors as it emits three fully resolved neutron lines [Miy03] (see Fig. 6).

The high energy of the first excited state in ^{132}Sn (4.041 MeV [Ker73]) makes neutron-gamma cascades energetically impossible for all but the states populated in Gamow-Teller transitions at high energies. For those cases the large difference in phase spaces favors neutron emission to the ground state. The presence of neutron transitions at energies smaller than 1 MeV would be indicative of population of the 2^+ state. In those cases, neutron-gamma coincidences using the clover array (1% efficiency at 4 MeV) will allow for correct identification of the neutron-emitting states.

Figure 4: (left) Schematic drawing of the IDS setup using four clovers combined with the IDSND detector and support at 1 m flight path. (right) picture of IDSND commissioning run for ISOLDE experiment IS609.

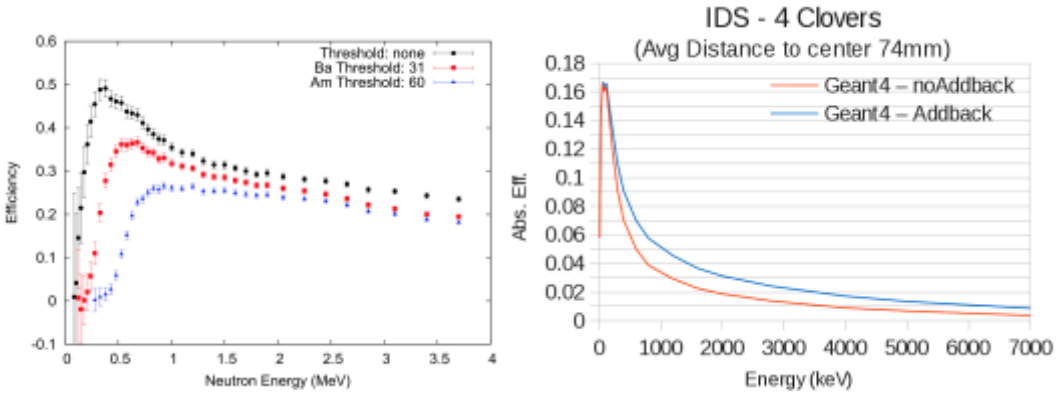

Figure 5: (left) Efficiency curves of IDSND, black points for the efficiency using the minimum threshold achievable by our electronics (~ 8 keV), red points with a threshold of 31 keV, and blue with a threshold of 60 keV. (right) Geant4 simulation of the efficiency of 4 IDS clovers up to 7 MeV. The curves were validated comparing with the efficiency obtained with a ^{152}Eu source.

Beam Request

Table 1 summarizes the requested beam time. Owing to the continuous development by the target and RILIS groups, a yield of 1000 ions/μC of ^{133}In has been recently demonstrated (experiment IS610 [Fra16]) using laser ion source with a hot Ta cavity. Narrowband laser ionization was later used in the same experiment to demonstrate isomer selectivity for ^{133}In. On-resonance yields were observed to be reduced by 20% for the ground state and a by a factor of 10 for the isomer compared to broadband ionization rates [Fra16]. Contamination from surface ionized ^{133}In can occur even when the ground-state or isomer are off-resonance. The off-resonance yields in both cases were estimated from ^{129}In measurement to be a factor 20 smaller than broadband yields [Goo16]. We assumed the same reduction factors for on/off-resonance ionization of ^{133}In in Table 1 and all simulations in this proposal. Isobaric contamination is expected to be small, and no other isobars have appreciable neutron branching ratios.

In order to calibrate the detector response, we request 1 shift of ^{17}N beam. Molecular extraction of ^{17}N using a CaO target was recently demonstrated at ISOLDE, with yields of 100 ions/μC (IS605).

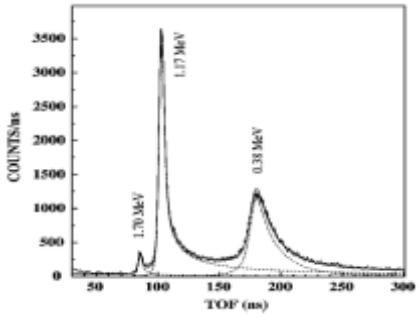

Figure 6: Neutron time of flight for beta decay of ^{17}N [Miy03]. The three resonances are fully resolved with a 100 cm flight path.

*Table 1: Expected neutron rates. The calculation is done for 2 uC PS Booster beam and 50% transmission efficiency to IDS. *The neutron branching ratio of the isomer is estimated from the log(ft) values of the sole two forbidden transitions populating neutron unbound states.*

	P_n (%)	Yield (ion/μC)	IDSND Eff	Neutrons (1/h)	Shifts	Target	Source
^{133}In ($9/2^+$)	80%	800	0.04	$1.5\ 10^5$	6	UC_X	Hot Ta line and cavity + RILIS
^{133}In ($1/2^-$)	4.75%*	100	0.04	1.010^3	6	UC_X	Hot Ta line and cavity + RILIS
^{17}N	95.1%	100	0.04	$1.8\ 10^4$	1	CaO	Hot Ta line and cavity

Summary of requested shifts:

We request 13 shifts to collect at least 10^6 neutrons from the decay of the ground state in ^{133}In. This will ensure that about 10^4 neutrons are detected from states populated in forbidden decay from both the ground state and 1/2- isomer. Recording at least 10^4 neutron events will ensure that these transitions can be measured in the presence of the tail of the neutrons emitted from the GT fed state. Beam time breaks down in 6 shifts with RILIS selecting the ground state and isomer respectively and 1 shift for ^{17}N calibration.

References:

[Als16] M. F. Alshudifat et al., Phys. Rev. C **93**, 044325 (2016)

[Ata15] D. Atanasov et al., Phys. Rev. Lett. **115**, 232501 (2015).

[Bin14] S. Binder, J. Langhammer, A. Calci, R. Roth. Phys. Lett. **B736**, 119 (2014).

[Bro14] B. A. Brown and W. D. M. Rae, Nucl. Data Sheets 120, 115 (2014).

[Fra77] H. Franz et al., Nucl. Instr. Meth. **144**, 253 (1977).

[Fra16] L.M. Fraile, ISOLDE HRS eLogBook, June 9th (2016).

[Goo16] T. Goodacre, private communication.

[Gre04] S. Grévy et al., Nucl. Phys. **A734**, 369 (2004).

[Hag16] G. Hagen, G. R. Jansen, and T. Papenbrock, Phys. Rev. Lett. (in print).

[Heb11] K. Hebeler et al., Phys. Rev. C **83**, 031301(R) (2011).

[Hof96] P. Hoff et al., Phys. Rev. Lett. **77**, 1020 (1996).

[Jon10] K.L. Jones et al., Nature **465**, 454 (2010).

[Jun16a] A. Jungclaus et al., Phys. Rev. C **93**, 041301(R) (2016).

[Jun16b] A. Jungclaus et al., Phys. Rev. C **94**, 024303 (2016).

[Ker73] A. Kerek , G.B. Holm, L.-E. De Geer, S. Borg, Phys. Lett. **B44,** 252 (1973).

[Lor15] G. Lorusso et al., Phys. Rev. Lett. **114**, 192501 (2015).

[Lic16] R. Licâ et al., Phys. Rev. C **93**, 044303 (2016).

[Mad16] M. Madurga et al., Phys. Rev. Lett. **117**, 092502 (2016).

[Miy03] H. Miyatake et al., Phys. Rev. C **67**, 014306 (2003).

[Mum16] M.R. Mumpower, R. Surman, G.C. McLaughlin, and A. Aprahamian, Prog. Part. Nucl. Phys. **86,** 86 (2016).

[Nac04] E. Nacher *et al*., Phys. Rev. Lett. **92**, 232501 (2004).

[Ots10] T. Otsuka et al., Phys. Rev. Lett. **104**, 012501 (2010).

[Pap16] T. Pappenbrock, private communication.

[Per06] F. Perrot et al., Phys. Rev. C **74**, 014313 (2006).

[Pet16] W. A. Peters et al., Nucl. Inst. Meth. **A836,** 122 (2016).

[Sin98] B. Singh et al., Nucl. Data Sheets **84**, 487 (1998).

[Tap14] J. Taprogge et al., Phys. Rev. Lett. **112**, 132501 (2014).

[Tap15] J. Taprogge et al. Phys. Rev. C **91**, 054324 (2015).

[Wat14] H. Watanabe et al. Phys. Rev. Lett. **113**, 042502 (2014).

[Wan12] M. Wang et al., Chin. Phys. **36**, 1603 (2012).

[Wie13] F. Wienholtz et al., Nature **498**, 346 (2013).

[Xu14] Z.Y. Zu et al., Phys. Rev. Lett. **113**, 032505 (2014).

[Zhi13] Q. Zhi et al., Phys. Rev. C **87**, 025803 (2013).

Appendix

DESCRIPTION OF THE PROPOSED EXPERIMENT

The experimental setup comprises: *(name the fixed-ISOLDE installations, as well as flexible elements of the experiment)*

Part of the Choose an item.	Availability	Design and manufacturing
[if relevant, name fixed ISOLDE installation: COLLAPS, CRIS, ISOLTRAP, MINIBALL + only CD, MINIBALL + T-REX, NICOLE, SSP-GLM chamber, SSP-GHM chamber, or WITCH]	☒ Existing	☒ To be used without any modification
	IDS + IDSND	
[Part 1 of experiment/ equipment]	☐ Existing	☐ To be used without any modification ☐ To be modified
	☐ New	☐ Standard equipment supplied by a manufacturer ☐ CERN/collaboration responsible for the design and/or manufacturing
[Part 2 experiment/ equipment]	☐ Existing	☐ To be used without any modification ☐ To be modified
	☐ New	☐ Standard equipment supplied by a manufacturer ☐ CERN/collaboration responsible for the design and/or manufacturing
[insert lines if needed]		

HAZARDS GENERATED BY THE EXPERIMENT

(if using fixed installation) Hazards named in the document relevant for the fixed [COLLAPS, CRIS, ISOLTRAP, MINIBALL + only CD, MINIBALL + T-REX, NICOLE, SSP-GLM chamber, SSP-GHM chamber, or WITCH] installation.

Additional hazards:

Hazards			
	[Part 1 of the experiment/equipment]	*[Part 2 of the experiment/equipment]*	*[Part 3 of the experiment/equipment]*
Thermodynamic and fluidic			
Pressure	[pressure] [Bar], [volume] [l]		
Vacuum			
Temperature	[temperature] [K]		

Heat transfer			
Thermal properties of materials			
Cryogenic fluid	[fluid], [pressure][Bar], [volume][l]		
Electrical and electromagnetic			
Electricity	[voltage] [V], [current][A]		
Static electricity			
Magnetic field	[magnetic field] [T]		
Batteries	☐		
Capacitors	☐		
Ionizing radiation			
Target material	[material]		
Beam particle type (e, p, ions, etc)			
Beam intensity			
Beam energy			
Cooling liquids	[liquid]		
Gases	[gas]		
Calibration sources:	☐		
• Open source	☐		
• Sealed source	☐ [ISO standard]		
• Isotope			
• Activity			
Use of activated material:			
• Description	☐		
• Dose rate on contact and in 10 cm distance	[dose][mSV]		
• Isotope			
• Activity			
Non-ionizing radiation			
Laser			
UV light			
Microwaves (300MHz-30 GHz)			
Radiofrequency (1-300MHz)			
Chemical			
Toxic	[chemical agent], [quantity]		
Harmful	[chemical agent], [quantity]		

CMR (carcinogens, mutagens and substances toxic to reproduction)	[chemical agent], [quantity]		
Corrosive	[chemical agent], [quantity]		
Irritant	[chemical agent], [quantity]		
Flammable	[chemical agent], [quantity]		
Oxidizing	[chemical agent], [quantity]		
Explosiveness	[chemical agent], [quantity]		
Asphyxiant	[chemical agent], [quantity]		
Dangerous for the environment	[chemical agent], [quantity]		
Mechanical			
Physical impact or mechanical energy (moving parts)	[location]		
Mechanical properties (Sharp, rough, slippery)	[location]		
Vibration	[location]		
Vehicles and Means of Transport	[location]		
Noise			
Frequency	[frequency],[Hz]		
Intensity			
Physical			
Confined spaces	[location]		
High workplaces	[location]		
Access to high workplaces	[location]		
Obstructions in passageways	[location]		
Manual handling	[location]		
Poor ergonomics	[location]		

0.1 Hazard identification

3.2 Average electrical power requirements (excluding fixed ISOLDE-installation mentioned above): *(make a rough estimate of the total power consumption of the additional equipment used in the experiment)*